Received: 15 July 2022 | Revised: 19 January 2023 | Accepted: 23 January 2023

DOI: 10.1002/nano.202200149

RESEARCH ARTICLE

Nano Select Open Access WILEY

Crucial interactions of functional pyrenes with graphite in electrodes for lithium-ion batteries

Marina Bauer[1] | **Philipp Konnerth**[2] | **Hannes Radinger**[1,3] | **Kristina Pfeifer**[1] | **Yug Joshi**[1] | **Felix Bauer**[1] | **Helmut Ehrenberg**[1] | **Frieder Scheiba**[1]

[1]Institute for Applied Materials, Karlsruhe Institute of Technology, Eggenstein-Leopoldshafen, Germany

[2]Department of Conversion Technologies of Biobased Resources, University of Hohenheim, Stuttgart, Germany

[3]Department of Chemical and Process Engineering, University of Canterbury, Christchurch, New Zealand

Correspondence
Frieder Scheiba, Institute for Applied Materials, Karlsruhe Institute of Technology,
Hermann-von-Helmholtz-Platz 1, 76344 Eggenstein-Leopoldshafen, Germany.
Email: frieder.scheiba@kit.edu

Abstract

Polycyclic aromatic hydrocarbons, such as pyrenes, are a well-known material class for non-covalent modification of carbon surfaces in many applications. In electrochemical energy storage, pyrenes are mostly used in large polymeric structures. This work addresses the use of carboxy- and amino-functionalized pyrenes for graphite electrodes for lithium-ion batteries (LIBs). Pyrenes are explored as adsorbed species on graphite prior to electrode fabrication and as additives to the electrode composition. Thereby, 1-pyrenecarboxylic acid, 1-pyrenebutyric acid, 1-aminopyrene, and 1-pyrenebutylamine were under investigation. As additives, pyrenes do not influence the cycling performance of the electrode at low current but deteriorate the performance at high current, regardless of the functional group. However, when the pyrenes are adsorbed to the graphite surface, the influence of the different functional groups becomes clearly visible, revealing that an additional butyl group has a positive impact on the cycling performance and lithium-ion transport of the electrodes. Electrodes with 1-pyrenebutyric acid even enhanced the performance compared to the pristine electrode.

KEYWORDS

additive, adsorbed, carbon surface, electrochemical performance, lithium-ion batteries, pyrenes

1 | INTRODUCTION

The surface of graphite electrodes in lithium-ion batteries (LIBs) plays an important role since it directly affects the formation of the solid-electrolyte interphase (SEI). Since the SEI influences the cycling stability of the battery, it is of great interest to understand how the surface can be tuned to improve the SEI formation and stability. Surface modification has proven useful for investigating the influence of functional groups on the SEI and the electrochemical performance of carbon electrodes for LIBs.[1–3] The reduction of *para*-substituted aryl diazonium salts is a common method for covalent surface modification,[4–6] where the functional groups are orientated perpendicular to the carbon surface. Pyrenes are a prominent example for non-covalent carbon surface modification, since they allow strong π–π interactions with sp^2-hybridized carbons due to their aromatic character.[7] Simple modification procedures and complete preservation of the substrate's aromatic system are reasons to choose pyrenes for surface modification. Various synthesis procedures have been described to attach diverse functional groups to the pyrene

structure, but several functionalized pyrenes can be purchased commercially as well. The non-covalent attachment of pyrenes to carbon surfaces has already led to great success concerning the dispersion of nanotubes[8–10] and conductivity tuning of graphene.[10,11] The use of pyrenes as electrolyte additive,[12] stabilizer of carbon nanotubes components,[13] surface modifiers for graphite felts,[14] or part of polymeric active materials[15–17] in energy storage systems has also been reported.

In this work, we focused on the adsorption of pyrenes containing carboxy and amino moieties on graphite. The native surface groups on graphite are of different nature (e.g., carboxylic, carbonyl, ether, hydroxyl) and heterogeneously distributed on the surface.[18] Since the pyrenes in this work provide one certain functional group, the influence of the corresponding functional group can be investigated selectively. The modified powders were used to prepare functionalized graphite electrodes for LIBs. The surface morphology was studied by scanning electron microscopy (SEM) and the electrochemical cycling performance at low (C/10) and high (1C) current reviewed in a three-electrode setup.

It is well-known that reducible surface groups can act as nucleation sites for the formation of the SEI.[19,20] Therefore, we expected reducible carboxy groups in 1-pyrenecarboxylic acid to show improved electrochemical behavior compared to non-reducible amino groups in 1-aminopyrene. Recently, we observed this trend to be true for functionalization of graphite electrodes with *p*-carboxy and *p*-amino aryl diazonium salts.[21] In contrast to aryl diazonium modification, the pyrene functional groups are orientated in parallel to the graphite surface. Additionally, we evaluated 1-pyrenebutyric acid and 1-pyrenebutylamine, where the functional groups are able to orientate either parallel to the basal plane or the edge site. We expect the functional groups in 1-pyrenebutyric acid and 1-pyrenebutylamine to be easier accessible as nucleation sites for SEI formation compared to 1-pyrenecarboxylic acid and 1-aminopyrene. Hence, the electrochemical performance of electrodes with butyl-containing pyrenes is expected to be superior to electrodes with 1-pyrenecarboxylic and 1-aminopyrene. Pristine pyrene was used as well to distinguish the influence of the pyrene structure from the influence of the functional groups. The chemical structures of the pyrenes and used methods are shown in Figure 1.

2 | RESULTS AND DISCUSSION

The surface of graphite powder was modified with pyrenes by stirring graphite in a solution of the corresponding pyrene in dimethyl sulfoxide (DMSO). The resulting powders were used for electrode preparation. For the sake of clarity, the functionalized pyrenes will be labeled as carboxy, amino, butylcarboxy, and butylamine (see Figure 1). The modified powders and electrodes are compared to an untreated graphite powder and electrode, which will be referred to as pristine graphite powder and electrode, respectively.

Figure 2A displays the SEM images of a pristine graphite electrode with carbon black particles as conductive additive decorated on top and in between graphite particles. The morphology of the graphite particles in the pyrene-modified electrode appears roughened in comparison to the pristine graphite electrode, which appears rather smooth (Figure 2B). In cyclic voltammetry, pyrene-modified graphite powders exhibit higher currents compared to pristine graphite powder (Figure 2C). This is in accordance with the literature, where enhanced double-layer capacitance is attributed to pyrenes used in supercapacitors.[17,22,23] The graphite powders containing functionalized pyrenes reveal higher currents compared to the pure pyrene and both graphite powders containing amino-functionalized pyrenes show distinct redox peaks at 0.41 and 0.37 V versus AgCl/Ag. This peak was described as pseudo capacitive behavior of aminopyrene-functionalized reduced graphene oxide.[24] Additionally, graphite powder was stirred in pure DMSO overnight prior to electrode preparation to investigate if the method itself has an impact on the electrochemical performance. The delithiation capacity of the pristine and with DMSO treated electrode are shown in Figure 2D. The difference in the first cycle capacity is less than 5 mAh g^{-1} with a retention of 99.8% and 96.8% for pristine and the DMSO sample, respectively. The capacity difference at 1C is less than 10 mAh g^{-1} with a retention of 70% and 71% for pristine and the DMSO sample, respectively. These values are within the standard deviation of the pristine electrode (see error bars), proving that the solvent does not influence the electrochemical properties of the electrodes.

Figure 2E displays the capacity values of pyrene-containing electrodes. It is clearly visible that the capacities are affected by the addition of pyrenes when compared to Figure 2D. Pyrenes, which carry functional groups, can indeed enhance the performance of graphite as it is observed in the case of the butylcarboxy electrode (Figure 2E). The following key information can be derived from Figure 2E: (1) pure pyrene electrodes provide the lowest capacity at low and high current; (2) electrodes containing pyrenes with carboxy groups provide higher capacities than electrodes containing pyrenes with amino groups, especially at high current; (3) electrodes containing butylcarboxy and butylamine provide higher capacities than electrodes containing carboxy and amine, respectively; (4) electrodes containing butylcarboxy provide comparable

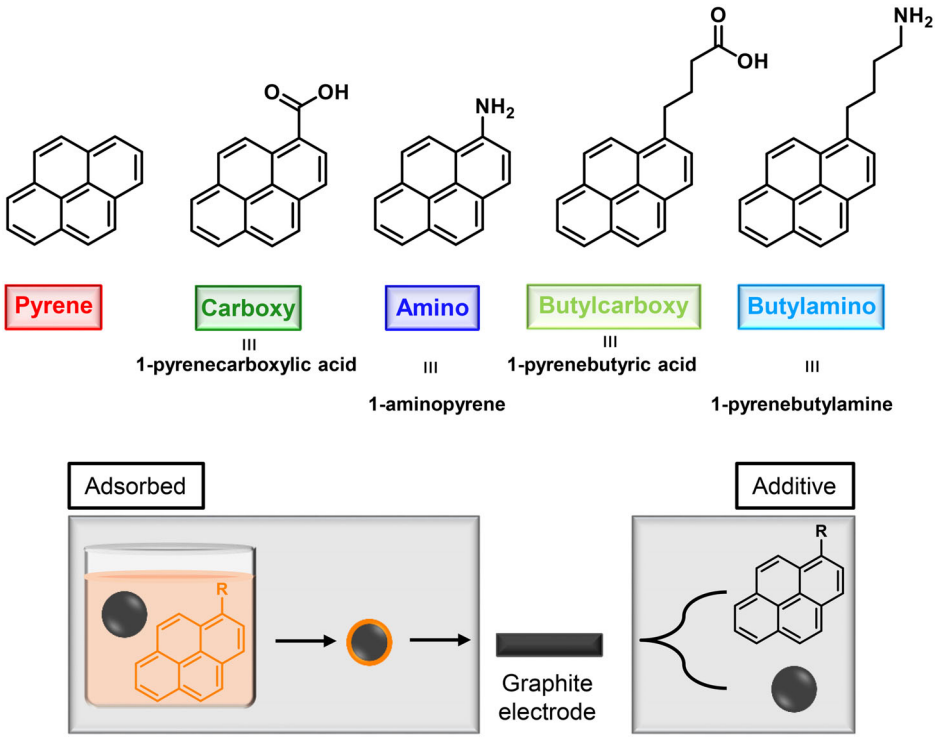

FIGURE 1 Chemical structures of the pyrenes and methods used in this work.

capacities to the pristine electrode at low current and even enhanced the capacity by 20 mAh g^{-1} at high current and the capacity retention by 18% compared to pristine. The trends (1)–(3) observed for the capacities are also valid for initial efficiencies, where electrodes containing pure pyrene show the lowest efficiency, electrodes containing carboxy groups reveal higher efficiencies than electrodes containing amino groups and electrodes containing functional groups with butyl groups show higher efficiencies than without (Figure 2F). Except for electrodes containing pure pyrene, for all modifications the Coulombic efficiency of the first cycle slightly increased. Compared to 87% for pristine graphite electrodes, butylcarboxy electrodes show an enhanced initial efficiency of 90%. For pure pyrene and amine electrodes, the capacity and efficiency at C/10 drops compared to the pristine graphite electrode. Due to the lack of functional groups, pure pyrene offers less active sites for SEI formation, which could lead to a less effective surface passivation.[19,20] Pure pyrene may even cover native surface oxygen groups of graphite rendering them inaccessible as anchor points during SEI formation. In contrast, the amino group offers an anchor group for SEI formation. Even though the amino group is not reducible, it is a nucleophilic substituent and changes the reactivity of the pyrene molecule. These aspects seem to positively influence the SEI formation and could explain the better performance compared to pure pyrene electrodes. However, the efficiencies of the pristine graphite electrode are still remarkably higher than those of the amine electrode, which suggests poor surface passivation in the first cycles. The butylamine electrode shows even higher capacities and efficiencies than the amine electrode. In general, carbon-carbon single bonds, as present in the butyl group, are able to freely rotate, which makes the amine group attached to the butyl group more flexible than the amine group, which is directly attached to the pyrene moiety.[25] Therefore, a possible explanation for the observed efficiencies could be that the addition of a butyl moiety indeed increases the accessibility of the amino group and hence positively influences the SEI formation. Further, the lone-pair of nitrogen in the amine sample is conjugated to the aromatic ring system of pyrene (+M-effect),[26] which is not the case for the butylamine sample. Additionally, the electron density of nitrogen is affected by the inductive effect (+I-effect)[26] of the butyl moiety. These effects make the butylamine sample more nucleophilic than the amine sample, which could lead to a better formation and anchoring of the SEI layer.

The efficiencies of butylcarboxy electrodes are within the error range of the pristine graphite electrodes, whereas carboxy electrodes show slightly decreased efficiencies. The capacities of the carboxy electrodes are comparable to the pristine graphite electrode, whereas the butylcarboxy electrodes clearly show enhanced capacities compared to the pristine graphite electrode. This is in line with the literature, where reducible surface oxygen groups are described

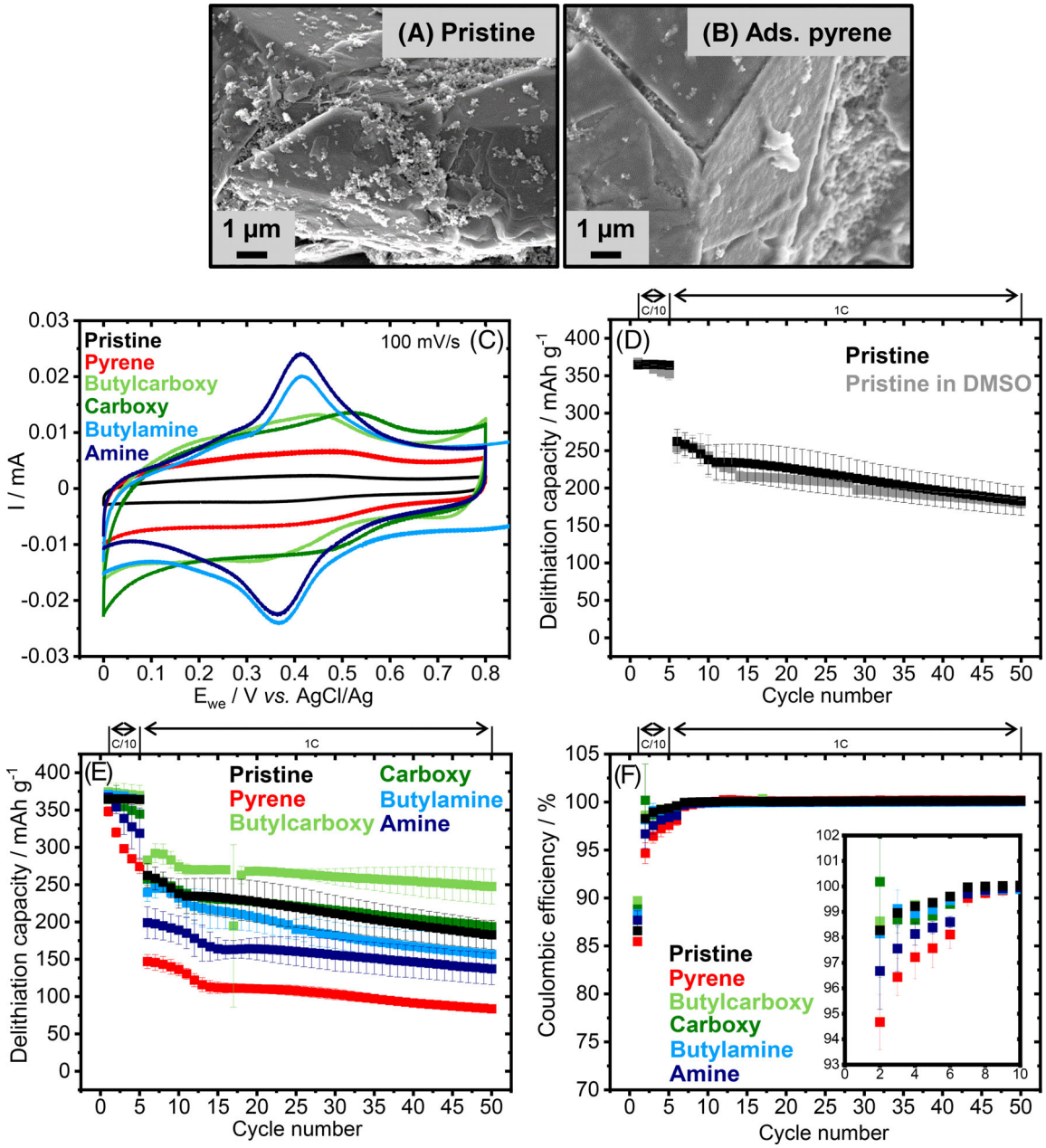

FIGURE 2 SEM images of (A) a pristine graphite electrode; (B) an electrode containing adsorbed pyrene; (C) CV of pristine and adsorbed pyrenes graphite powders; (D) electrochemical cycling stability of pristine and with dimethyl sulfoxide (DMSO) treated electrodes; (E) electrochemical cycling stability at C/10 for 5 cycles and 1C for 45 cycles; and (F) corresponding Coulombic efficiencies of pristine and adsorbed pyrenes electrodes.

to function as nucleation sites for the formation of a stable SEI,[19,20] which could also explain the superior performance of electrodes with reducible carboxy groups compared to non-reducible amino groups. The positive effect of the additional butyl group could also stem from the better steric accessibility of the carboxy group in the butylcarboxy sample.

We assume that the pyrenes do not just act as additives providing certain functional groups and being consumed during the SEI formation, but that it is essential that they are adsorbed to the graphite surface to provide a beneficial contribution to the formation and stability of the SEI layer. To investigate this assumption, 1% w/w pyrene, amino, butylamino, carboxy, and butylcarboxy powders were added as additive to a graphite electrode. The modified electrodes are again compared to an untreated graphite electrode, which will be referred to as pristine graphite electrode.

The SEM image of an electrode with 1% w/w pyrene is compared to an SEM image of the pristine graphite

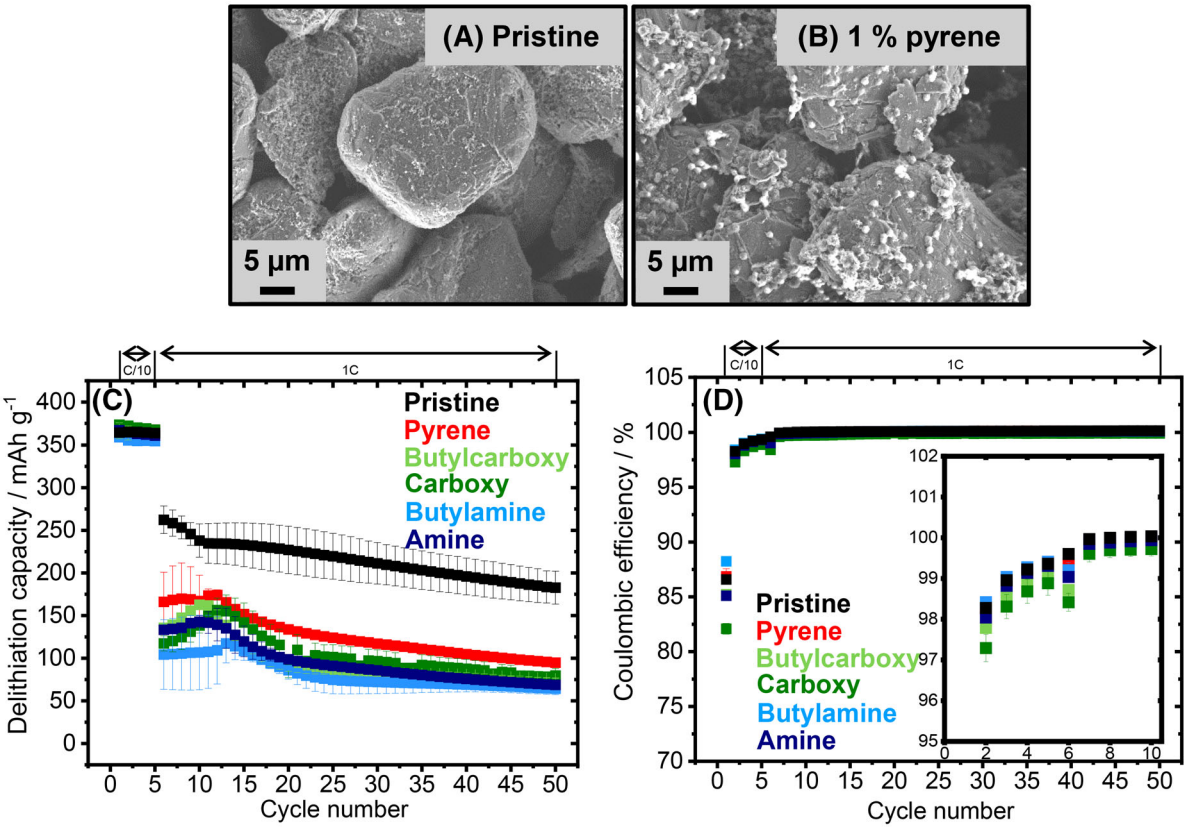

FIGURE 3 SEM images of (A) a pristine graphite electrode, (B) an electrode containing 1% w/w pyrene as additive, (C) electrochemical cycling stability at C/10 for 5 cycles and 1C for 45 cycles, and (D) corresponding Coulombic efficiencies of pristine electrodes and electrodes with 1% w/w pyrenes as additives.

electrode in Figure 3A,B. The 1% w/w pyrene electrode shows an equal distribution of spherical pyrene particles, which are attached to graphite and conductive carbon (Figure 3B). Pyrene particles are also attached to each other forming a network around graphite. The electrochemical cycling performance and Coulombic efficiencies are displayed in Figure 3C,D. The capacity values of electrodes containing pyrene additives at a cycling rate of C/10 are comparable to the pristine graphite electrode, whereas their capacity visibly drops at 1C. Electrodes containing pure pyrene perform best at 1C among all pyrene-containing electrodes, exhibiting delithiation capacities of 166–95 mAh g^{-1} at 1C. The lowest capacities of 104–64 mAh g^{-1} were obtained using butylamine as additive at 1C. The presence of pyrene particles does not seem to notably influence the capacity of the electrode at C/10 in contrast to 1C where the capacity drops by at least 37% compared to the pristine. The Coulombic efficiency in the first cycle of the pure pyrene-containing electrode is equal to the pristine graphite electrode (87%). For electrodes with butylamine additive the efficiency of the first cycle is enhanced by 1%, while electrodes with amine and butylcarboxy additive show efficiencies reduced by about 2%. The efficiency of electrodes with carboxy additive is even further reduced by about 5%. In the following cycles, especially the electrodes with carboxy additive show decreased efficiencies compared to the pristine graphite electrode. It is notable that the efficiency of electrodes with butylamine additive is superior to electrodes with amine additive and the efficiency of electrodes with butylcarboxy additive is superior to carboxy additive.

Regardless of the functional group, the cycling performances of the electrodes with pyrenes as additive are deteriorated at high current, but do not seem to influence the performance at low current. The presence of aggregated pyrene particles on the graphite surface (see Figure 3B) seems to have a significant contribution to the inner resistance at high current. However, this contribution appears to be neglectable at low current, because under these conditions graphite offers sufficient electronic pathways due to its higher conductivity compared to pyrene.[27–30] Another explanation could be that the pyrene agglomerates act as local nucleation sites, leading to a SEI with inferior properties compared to the pristine graphite. Therefore, pyrenes as additive seem not to support anchoring of SEI components to the graphite surface during growth. In addition, the pyrenes are at least partly soluble in the electrolyte so that they could dissolve

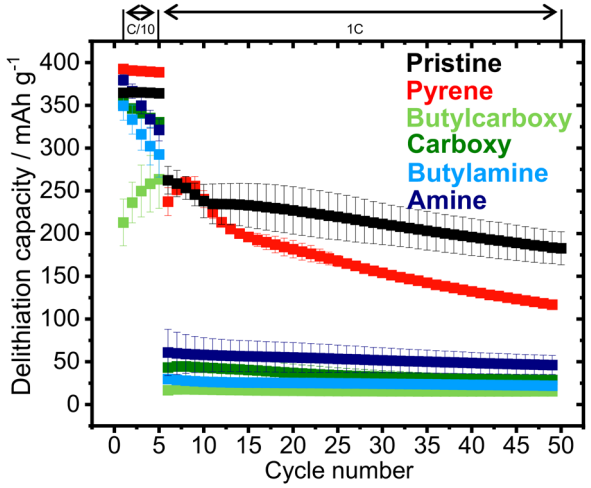

FIGURE 4 Electrochemical cycling stability at C/10 for 5 cycles and 1C for 45 cycles for pristine electrodes and electrodes with 5% w/w pyrenes as additives.

and directly interfere with the SEI formation process again resulting in an inferior SEI.

Considering 1 g of electrode, graphite with pyrenes as additives contains 10 mg of pyrene, whereas graphite with adsorbed pyrenes from a 5 mM solution contains at maximum 51–72 mg of pyrene (fluctuation due to different molar masses of functional pyrenes). In order to exclude a concentration effect, we prepared electrodes with 5% w/w pyrene additives. In this case, 1 g of electrode contains 50 mg of pyrene additive.

Figure 4 shows that by increasing the additive content in the electrodes to 5% w/w, the delithiation capacities of the butylacid, acid, butylamine, and amine additive electrodes deteriorate already at C/10, which was not the case for electrodes with 1% w/w of pyrenes (see Figure 3C). Furthermore, the capacities at 1C are even lower compared to electrodes with 1% w/w of pyrenes. This reinforces that the sole presence of butylacid pyrene powder in the electrode is not decisive for the superior performance in Figure 2C and that it is not a matter of proportion either. However, the electrodes containing 5% w/w of pure pyrene show higher capacities at C/10 compared to the pristine graphite electrode and higher capacities at 1C compared to the corresponding electrodes containing adsorbed pure pyrene and 1% w/w pure pyrene as additive in Figures 2E and 3C, respectively. The reason for this effect is not clear, but since pyrene without functional groups only functions as a comparative sample in this study, the evaluation of this observation will not be discussed further.

The differential capacity was calculated and plotted versus voltage to further investigate the electrochemical behavior of pyrenes in the adsorbed and 1% w/w electrodes in the first and 10th cycle (Figure 5A–D). The reduction peak at ~0.7 V in the first cycle is ascribed to the reduction of ethylene carbonate (EC)[31] and is visible for all samples (Figure 5A,C, insets). As an additive, butylcarboxy, butylamine, and amine electrodes show an additional reduction peak at 0.9 V and carboxy at 1.2 V (Figure 5C, inset). The two reduction peaks are most pronounced for carboxy additive electrodes, which is in correlation with the low first-cycle efficiency. Pyrene additive electrodes do not show an additional peak in this area, which makes it plausible that those peaks are linked to reactions with the functional groups. However, except for butylamine additive electrode those peaks are not visible for electrodes with adsorbed pyrenes (Figure 5A, inset). The EC reduction peak of the electrodes with adsorbed pyrenes did neither shift nor change in intensity, except for butylamine electrodes, where the peak intensity increased. A possible explanation for this observation could be the different amounts of pyrenes in the electrode due to different modification methods, assuming there is a smaller amount of adsorbed pyrenes and hence the absence of the additional peaks. However, those peaks in the insets of Figure 5C for additive electrodes seem to arise from additional irreversible reactions with the pyrenes itself and may not be connected to the electrolyte reduction reactions.

In the first cycle (C/10), the difference between the reduction and oxidation peaks of all electrodes containing adsorbed pyrenes is lowered, indicating either an enhanced lithium-ion transport or increase in the electronic conductivity (reduction in charge transfer resistance) (Figure 5A). In the 10th cycle (1C), it is noticeable that for the adsorbed variant (Figure 5B) for butylcarboxy and butylamino electrodes the reduction peaks between 0.01 and 0.1 V versus Li^+/Li have a significantly higher charge exchange (i.e., dQ) per voltage change compared to the carboxy, amino, pyrene, and the pristine graphite electrodes. This would also point to a faster ionic migration. This is especially noticeable in the case of butylcarboxy electrodes which show sharp and intense peaks in the 10th cycle. Figure 5B reassures the positive influence of the additional butyl group in the functionalized pyrene samples.

The reduction peaks of the first cycle at C/10 for electrodes with pyrene additives are slightly shifted to higher potentials for all samples except butylamine additive electrodes (Figure 5C). However, at 1C, the peak shift to lower/higher potentials and decreased peak heights during reduction/oxidation indicates the lithium-ion transport is deteriorated for all samples (Figure 5D). This affirms that the influence of aggregated pyrenes on the inner resistance only becomes significant at high current.

To elucidate the observed behavior for electrodes with adsorbed pyrenes, electrochemical impedance spectroscopy (EIS) was conducted on symmetrical cells at

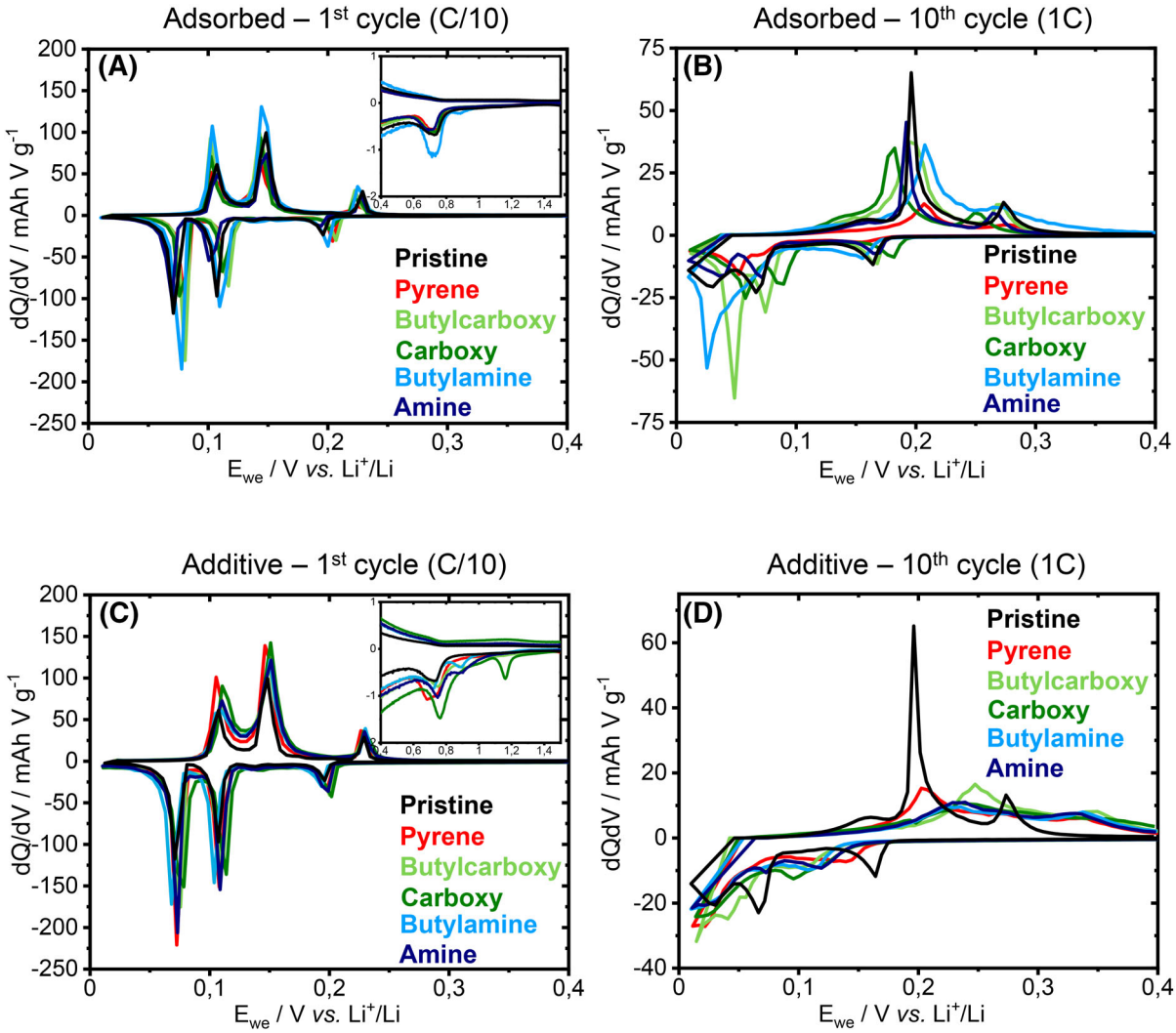

FIGURE 5 dQ/dV plots of the first (C/10) (A) and 10th (1C) cycle (B) of pristine and adsorbed pyrenes electrodes and first (C/10) (C) and 10th (1C) cycle (D) of pristine and pyrenes as additive electrodes.

0.01 V versus Li^+/Li. Figure 6A shows the corrected Nyquist plot (the data is shifted in x-axis to correct for the internal resistances of the connecting wires, the raw data is shown in Figure S1). From the inset of Figure 6A, the magnified region of the Nyquist plot, it is clear that the charge-transfer resistances (the intercept of the semicircle on the x-axis) is lowered upon surface modifications by carboxy and butylcarboxy pyrenes. The effect is much more prominent in the case of butylcarboxy. To extract more information from the impedance curves, the Nyquist plots were modeled using the circuit shown in Figure 6B. The model has a Randel's circuit element consisting of a modified Warburg element for the finite diffusion layer (M_{a2}), constant phase element (Q2), and a resistance (R2). Additionally, a constant phase element (Q3) and resistance (R3) were added to the model-circuit for the tailing of the Nyquist plot in the low-frequency regime. A representative fit of the pristine graphite electrode is shown in Figure 6B. The same model was used to fit all the plots. The corresponding fitting parameters and the fitted curves are given in the supplementary (Figure S2). From the fitting parameters, the charge transfer resistance (R_{ct} or R_2) and Warburg impedance (corresponding to the M_{a2}) are obtained. The corresponding diffusion coefficients were extracted from the Warburg impedance.[32] The R_{ct} for the pristine, carboxy, and butylcarboxy electrodes corresponds to 5.461, 5.405, and 4.761 Ω, respectively. Moreover, the diffusion coefficient for the pristine, carboxy and butylcarboxy electrodes corresponds to 5.53×10^{-11} cm^2 s^{-1}, 6.61×10^{-11} cm^2 s^{-1}, and 8.14×10^{-11} cm^2 s^{-1}, respectively. The obtained diffusion coefficients are in the range reported for Graphite 10^{-9} to 10^{-12} cm^2 s^{-1}.[33–36] The exact comparison between different studies is difficult as the diffusion coefficients depend on a lot of factors but their comparison within this study for differently modified graphite is definitely possible. From the evaluated data, it is

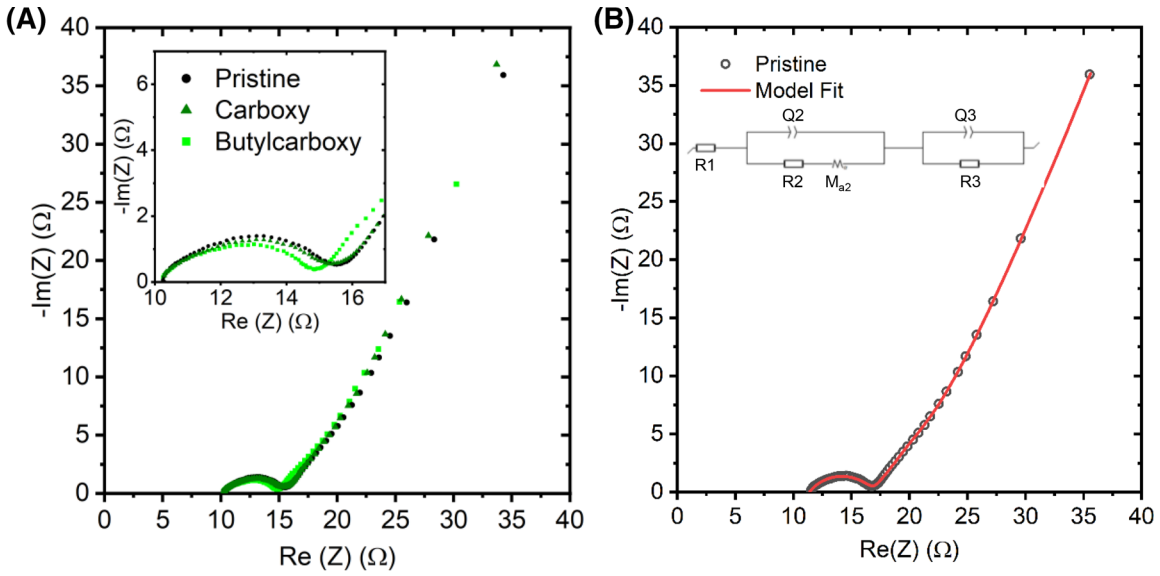

FIGURE 6 Corrected Nyquist plots of the pristine and adsorbed carboxy and butylcarboxy pyrene electrodes (A) and model fit and circuit of the pristine electrode (B).

clear that surface modification of the pristine graphite with carboxy and butylcarboxy pyrene results in the reduction of the charge-transfer resistance as well as an increase in the diffusion of lithium into the bulk of the electrode. Both of these will result in the reduction of the overpotential as observed in dQ/dV plots in Figure 5A,B. Furthermore, the enhanced diffusion coefficient could only be understood if the interface of the electrode is controlling the diffusional flux of lithium as the bulk diffusion of lithium should be the same for graphite irrespective of the surface. This points to the fact that either the SEI is getting modified, or the surface groups reduce the activation barrier for the interfacial transport. However, the evaluation of the exact mechanism of lithium transport through the interface is beyond the scope of this work but could be the focus of a future work. Nevertheless, the study clearly highlights the beneficial effects of the surface modification by functionalized pyrenes (more specifically by butylcarboxy) and differentiates it from the mere addition of the pyrenes as additives.

3 | CONCLUSION

In summary, we studied pyrenes with carboxy and amino moieties for graphite electrodes in LIBs. When the pyrenes are adsorbed to the graphite surface, different influences of the functional groups are visible. Our assumptions that carboxy groups are superior to amino groups and that butylcarboxy/butylamine are superior to carboxy/amine were confirmed. The additional butyl moieties change the reactivity and steric accessibility of the pyrenes and functional groups, which seems to have a positive impact on the SEI formation. Butylcarboxy even showed an improved cycling performance and better lithium-ion transport compared to a pristine graphite electrode. Such improving effect did not appear for the application of pyrenes as additive, proving that it is crucial to have surface adsorbed pyrenes.

4 | EXPERIMENTAL SECTION

4.1 | Surface modification

4.1.1 | General procedure for adsorption of pyrenes

1 g graphite was added to a 5 mM solution of the corresponding pyrene in 50 mL DMSO. After stirring overnight, the dispersion was filtered and washed thoroughly with DMSO. All powders were dried under vacuum and used for electrode preparation as described below.

4.2 | Cyclic voltammetry of pyrene-modified graphite powders

The modified graphite powders were dropcasted on a glassy carbon electrode. The glassy carbon electrode was used as working electrode, a graphite rod electrode as counter electrode and AgCl/Ag as reference electrode. The cyclic voltammetry was performed in H_2SO_4 with a scan rate of 100 mV s^{-1}.

4.3 | Scanning electron microscopy

Scanning electron microscopy was conducted using a thermal field emission scanning electron microscope (FESEM, Carl Zeiss SMT AG) at an acceleration voltage of 5 kV. The samples were fixed on a steel sample holder by using sticky tape.

4.4 | Electrode preparation

90% w/w graphite (Mechano-Cap 1P1, H.C. Carbon) and 3% w/w conductive additive C65 (C-NERGY) were ground prior to dry-mixing at 1000 rpm in a speedmixer (DAC150.1 FVZ, Hauschild). DMSO was added dropwise, and the dispersion was mixed at different speeds between 1500 and 3000 rpm before 7% w/w polyvinylidene fluoride (PVdF) binder dissolved in DMSO was added. Mixing the dispersion for 10 minutes at 800 rpm gave a viscous paste that was subsequently coated on copper foil with a doctor blade (wet thickness 200 μm). The coating was dried at room temperature overnight, at 120°C for 8 hours and finally at 120°C in vacuum overnight.

The composition for electrodes with pyrenes as additive were 89% w/w graphite, 1% w/w pyrene, 3% w/w C65 and 7% w/w PVdF, and 85% w/w graphite, 5% w/w pyrene, 3% w/w C65 and 7% w/w PVdF, respectively.

4.5 | Cell assembly

Electrochemical measurements were performed in three-electrode setups in custom-built polyether ether ketone (PEEK) cells with spring loaded titanium pistons as described in ref [37]. Cell assembly was performed in an Ar-filled glovebox. Working electrodes were punched to 12 mm discs and were separated from the 12 mm lithium metal counter electrode discs by a 13 mm glass fiber separator (GF/D, Whatman). Lithium metal was used as reference electrode. The cells were filled with 1 M $LiPF_6$ in a 50:50 mixture of EC and dimethyl carbonate (DMC) electrolyte (LP30, BASF).

4.6 | Electrochemical measurements

All measurements were carried out with the test cells in climate chambers at 25°C using a VMP3 potentiostat (Biologic). Galvanostatic Cycling with Potential Limitation (GCPL) measurements were performed between 0.01 V and 1.80 V versus Li^+/Li with C/10 for 5 cycles followed by 45 cycles with 1C. Prior to EIS, two electrodes per sample were lithiated with C/10 to 0.01 V using GCPL in a three-electrode setup as described above with an additional Cellgard separator between the graphite electrode and the glass fiber separator. After holding the potential at 0.01 V for 10 hours, the cells were disassembled and the two lithiated graphite electrodes were reassembled in a symmetrical two-electrode Swagelok cell. The cells were allowed to relax at open-circuit voltage for 1 hour before impedance spectra were acquired in the range 1 MHz to 3 mHz with a sinus amplitude of 5 mV.

ACKNOWLEDGMENTS

This work contributes to the research performed at CELEST (Center for Electrochemical Energy Storage Ulm-Karlsruhe). We acknowledge the SFB 1176 funded by the German Research Foundation (DFG) in the context of project B2 for funding. M.B. thanks Dr. Günter Staufer and Ramon Zimmermanns for useful discussion and Dr. Angelina Sarapulova, Tria Malliaridou, and Mattes Renner for support for electrochemical testing. H.R. thanks the Federal Ministry of Education and Research (BMBF) within the project Flow3DKat (03EK3053C) for financial support.

CONFLICT OF INTEREST

The authors declare no conflict of interest.

DATA AVAILABILITY STATEMENT

The data that support the findings of this study are available from the corresponding author upon reasonable request.

REFERENCES

1. J. Asenbauer, T. Eisenmann, M. Kuenzel, A. Kazzazi, Z. Chen, D. Bresser, *Sustain. Energy Fuels* **2020**, *4*, 5387.
2. X. Gong, Y. Zheng, J. Zheng, S. Cao, H. Wen, B. Lin, Y. Sun, *ChemElectroChem* **2020**, *7*, 1465.
3. L. J. Fu, H. Liu, C. Li, Y. P. Wu, E. Rahm, R. Holze, H. Q. Wu, *Solid State Sci.* **2006**, *8*, 113.
4. P. Verma, P. Novák, *Carbon 50* **2012**, *7*, 2599.
5. Q. Pan, H. Wang, Y. Jiang, *J. Mater. Chem.* **2007**, *17*, 329.
6. D. S. Moock, S. O. Steinmüller, I. D. Wessely, A. Llevot, B. Bitterer, M. A. R. Meier, S. Bräse, H. Ehrenberg, F. Scheiba, *ACS Appl. Mater. Interfaces* **2018**, *10*, 24172.
7. Y. Zhang, C. Liu, W. Shi, Z. Wang, L. Dai, X. Zhang, *Langmuir* **2007**, *23*, 7911.
8. K. C. Etika, F. D. Jochum, M. A. Cox, P. Schattling, P. Théato, J. C. Grunlan, *Macromolecules* **2010**, *43*, 9447.
9. K. C. Etika, F. D. Jochum, P. Théato, J. C. Grunlan, *J. Am. Chem. Soc.* **2009**, *131*, 13598.
10. J. Luan, A. Zhang, Y. Zheng, L. Sun, *Compos. Part A* **2012**, *43*, 1032.
11. J. Liu, R. Wang, L. Cui, J. Tang, Z. Liu, Q. Kong, W. Yang, J. Gooding, *J. Phys. Chem. C.* **2012**, *116*, 17939.

12. H. Shang, G. Peng, W. Liu, H. Zhang, W. Niu, Y. Liao, M. Qu, Z. Xie, *Energy Technol.* **2020**, *8*, 2000671.
13. W. Liu, Y. Hu, Y. Qiao, J. Jiang, M. Huang, M. Qu, G. Peng, Z. Xie, *Solid State Ionics* **2021**, *369*, 115724.
14. H. Radinger, A. Ghamlouche, H. Ehrenberg, F. Scheiba, *J. Mater. Chem. A.* **2021**, *9*, 18280.
15. T. Nokami, T. Matsuo, Y. Inatomi, N. Hojo, T. Tsukagoshi, H. Yoshizawa, A. Shimizu, H. Kuramoto, K. Komae, H. Tsuyama, J. Yoshida, *J. Am. Chem. Soc.* **2012**, *134*, 19694.
16. H. Wang, Z. Li, Z. Meng, X. Guo, Y. Du, H. Yang, *New J. Chem.* **2021**, *45*, 7060.
17. S. Bandyopadhyay, C. Singh, P. Jash, H. M. Waseem, A. Paul, A. Patra, *Chem. Commun.* **2018**, *54*, 6796.
18. M. E. Spahr, *Lithium-Ion Batteries*, Springer, New York **2009**, 127.
19. C. Mao, M. Wood, L. David, S. J. An, Y. Sheng, Z. Du, H. M. Meyer III, R. E. Ruther, D. L. Wood III, *J. Electrochem. Soc.* **2018**, *165*, A1837.
20. S. H. Ng, C. Vix-Guterl, P. Bernardo, N. Tran, J. Ufheil, H. Buqa, J. Dentzer, R. Gadiou, M. E. Spahr, D. Goers, P. Novák, *Carbon N. Y.* **2009**, *47*, 705.
21. M. Bauer, K. Pfeifer, X. Luo, H. Radinger, H. Ehrenberg, F. Scheiba, *ChemElectroChem* **2022**, *9*, e202101434.
22. S. Ghosh, X. An, R. Shah, D. Rawat, B. Dave, S. Kar, S. Talapatra, *J. Phys. Chem. C* **2012**, *116*, 20688.
23. J. D. Velásquez, M. Tomczykowa, M. E. Plonska-Brzezinska, M. N. Chaur, *Materials (Basel)*. **2020**, *13*, 1141.
24. E. Y. L. Teo, H. N. Lim, R. Jose, K. F. Chong, *RCS Adv*. **2015**, *5*, 38111.
25. D. Shubert, J. Leyba, *Chemistry and Physics for Nurse Anesthesia*, 2nd ed., Springer, New York **2013**.
26. B. S. Bahl, A. Bahl, *A Textbook of Organic Chemistry*. S. Chand Publishing, New Delhi **2017**.
27. A. Celzard, J. F. Marêché, F. Payot, G. Furdin, *Carbon N. Y.* **2002**, *40*, 2801.
28. N. Deprez, D. S. McLachlan, *J. Phys. D Appl. Phys.* **1988**, *21*, 101.
29. R. J. Waltman, *J. Electroanal. Chem.* **1985**, *194*, 49.
30. D. C. Northrop, O. Simpson, *Proc. R. Soc. Lond. A* **1956**, *234*, 124.
31. R. Imhof, P. Novák, *J. Electrochem. Soc.* **1998**, *145*, 1081.
32. T. Piao, S.-M. Park, C.-H. Doh, S.-I. Moon, *J. Electrochem. Soc.* **1999**, *146*, 2794.
33. A. Funabiki, M. Inaba, Z. Ogumi, *J. Electrochem. Soc.* **1998**, *145*, 172.
34. H. Yang, H. J. Bang, J. Prakash, *J. Electrochem. Soc.* **2004**, *151*, A1247.
35. M. D. Levi, E. Markevich, D. Aurbach, *J. Phys. Chem. B* **2005**, *109*, 7420.
36. J. H. Park, H. Yoon, Y. Cho, C.-Y. Yoo, *Materials (Basel)*. **2021**, *14*, 4683.
37. D. Weingarth, M. Zeiger, N. Jäckel, M. Aslan, G. Feng, V. Presser, *Adv. Energy Mater.* **2014**, *4*, 1400316.

SUPPORTING INFORMATION

Additional supporting information can be found online in the Supporting Information section at the end of this article.

How to cite this article: M. Bauer, P. Konnerth, H. Radinger, K. Pfeifer, Y. Joshi, F. Bauer, H. Ehrenberg, F. Scheiba, *Nano Select*. **2023**, *4,* 278. https://doi.org/10.1002/nano.202200149